tive. In an optical transition from a compact ground state, which is assumed inside the vacancy, only the part of the excited state which has overlap with the ground state is important. That part of the excited-state orbital has a positive angular momentum and determines the optical selection rule. On the other hand, the angular momentum of the state as a whole, which has a negative angular momentum, determines the Zeeman splitting of the state. The transition probability is therefore due to a function behaving as $x+iy$, but the Zeeman splitting of the state is determined by a function behaving as $x-iy$. The g value is therefore negative.

VI. DISCUSSION AND CONCLUSIONS

It appears possible to give a logical interpretation of the negative g value. It is also possible to reconcile such a negative g value with the symmetry assignment of $^1A_{1g} - {}^1T_{1u}$ for the optical transition. However, a rigid classification as $^1S - {}^1P$ based upon atomiclike wave functions transforming as spherical harmonics would be incompatible with the observed negative g value. The negative g value requires a large admixture of higher-order spherical harmonics such as those from an atomic F state. Whereas a $T_{1u}(P)$ state would have $g=1$, a $T_{1u}(F)$ state would have $g=-\frac{3}{2}$.

The observed negative g value is probably evidence for a much more diffuse excited state than has been found for the one-electron alkali-halide F centers where g values are positive. It can be speculated that the more diffuse state is a result of the more covalent nature and the relatively higher dielectric constant of CaO. A diffuse excited state might therefore also be expected in other alkaline-earth oxides. The excited states of the one-electron F^+ centers are certain to be more tightly bound. However, a very low orbital g value has been reported for the F^+ center in SrO,[10] and a lesser tendency toward a diffuse excited state might also explain this.

*Research sponsored by the U. S. Atomic Energy Commission under contract with the Union Carbide Corporation.

[1]J. C. Kemp, J. C. Cheng, E. H. Izen, and F. A. Modine, Phys. Rev. 179, 818 (1969).

[2]R. G. Bessent, B. C. Cavenett, and I. C. Hunter, J. Phys. Chem. Solids 29, 1523 (1968).

[3]Y. Merle d'Aubigne and A. Roussel, Phys. Rev. B 3, 1421 (1971).

[4]For a review see *Physics of Color Centers*, edited by W. Beall Fowler (Academic, New York, 1968).

[5]S. N. Jasperson and S. E. Schnatterly, Rev. Sci. Inst. 40, 761 (1969).

[6]B. Henderson, S. E. Stokowski, and T. C. Ensign, Phys. Rev. 183, 826 (1969).

[7]B. Henderson, Y. Chen, and W. A. Sibley, Phys. Rev. B 6, 4060 (1972).

[8]C. H. Henry, S. E. Schnatterly, and C. P. Slichter, Phys. Rev. 137, A583 (1965).

[9]D. Y. Smith, Phys. Rev. 183, A574 (1965).

[10]F. A. Modine, E. H. Izen, and J. C. Kemp, Phys. Letters 34A, 413 (1971).

PHYSICAL REVIEW B VOLUME 7, NUMBER 4 15 FEBRUARY 1973

Optical Properties of Dilute Solid-Rare-Gas Mixtures in the Extreme Ultraviolet

R. Haensel,* N. Kosuch,* U. Nielsen,* U. Rössler,† and B. Sonntag*
Deutsches Elektronen-Synchrotron DESY, Hamburg, Germany
(Received 23 June 1972)

The absorption spectra of thin films of mixtures of the rare gases Xe, Kr, Ar, and Ne have been measured in the photon range 40 — 260 eV, i.e., in the region of Ne-2s, Ar-2p, Kr-3d, and Xe-4d transitions. In most cases a continuous shifting of the energetic position of the absorption peaks of the pure-rare-gas solids upon addition of another rare gas of of N_2 can be observed, thus indicating a dilute mixing of both components over the whole range of concentrations. The shift of the absorption peaks can be understood in terms of the conduction-band density of states of pure-rare-gas solids.

I. INTRODUCTION

In the past few years the investigation of the optical properties of solid rare gases in the extreme ultraviolet[1-4] has gained much interest. Since the rare gases can be studied in a relatively easy way, both in the gaseous and in the solid state, common and different features of the optical properties of both states can be disentangled by comparing the spectra over a wide spectral range. The optical spectra of gaseous and solidified rare gases have common extended maxima, which are typical for the continuum absorption but differ in the fine structure at the threshold energies where electrons from the different core shells can be excited.

The continuum absorption of rare gases, with a broad maximum typical at energies several tens of electron volts above the threshold energy (delayed

$d \rightarrow f$ transitions) is well understood with the help of atomic theories. Photoionization cross sections, as calculated from realistic Hartree–Fock potentials for a single-particle model,[5–7] gave a good qualitative description of the experimental results. Recent calculations,[8–11] that include exchange and correlation terms, have improved agreement between the atomic model and the experiment. The characteristics of the continuum absorption have also recently been explained, from a solid state point of view,[12] as being due to a lack of orthogonalization corrections on the dipole matrix elements for $d \rightarrow f$ transitions.

The fine structure in the optical spectra of solid rare gases at the onset of transitions from the valence band has been studied for several years.[13–16] Experiments that have been performed with the help of LiF substrates[13–15] were restricted to photon energies smaller than 10.5 eV because of the short-wavelength cutoff of this material. This restriction was overcome by Baldini,[16] who used a cooled sapphire rod coated with a phosphor for the detection of ultraviolet light and directly evaporated the solid-rare-gas films onto this rod. He extended the accessible energy range up to 14 eV, the limit being due to his radiation source. The energy range was finally extended to 500 eV using synchrotron radiation as an ultraviolet source.[17,18] Besides transitions from the valence bands,[19–21] transitions from different core shells have also been studied.[1–4,22,23] Additional absorption measurements on solid Ne have been performed between 17 and 21 eV in the region of the valence-band transitions by Boursey *et al.*[24] using a triggered-vacuum-spark uranium-rod source.[25] In the hard x-ray region the K-absorption spectra of solid Ar and Kr have been measured by Soules and Shaw.[26] Besides the optical measurements, energy-loss experiments have been performed.[27–32]

An interpretation of the fine structure at the onset of transitions from the valence shell has been attempted in connection with energy-band calculations for solid rare gases carried out by several authors.[33–42] In these interpretations the general custom is to ascribe structures in the absorption spectrum to critical points in the joint density of valence- and conduction-band states. This procedure, which is very useful in the interpretation of optical spectra of semiconductors, is not quite correct in the case of insulators. As the valence electrons are tightly bound to the ions (the energy gap in solid rare gases being of the order of 10 eV), the electrons are not able to screen the Coulomb interaction between the excited electron and the hole which it leaves behind in the valence band. Thus, excitonic structures due to bound states of the electron-hole pair appear as hydrogenlike series[43] in front of the interband continuum. In addition, the Coulomb interaction is responsible for fluctuations in the density-of-states continuum.[44] It has, however, been pointed out that the density-of-states curves of the conduction bands[45] are useful in the interpretation of the fine structure in the absorption curves at the onset of core-shell transitions.[1–4]

A study of the absorption spectra of solid solutions of rare gases in the extreme ultraviolet yields a further check on the interpretation given to these spectra of pure solid rare gases and thus promotes the understanding of core-transition spectra in terms of electron states. Preliminary results of such experiments have already been reported elsewhere.[2–4] The measurements discussed in this paper were performed on binary mixtures of all rare gases and of N_2 for different concentrations c of the constituents. The energy range was between 40 and 260 eV. Since this energy range is above the ionization limit of all rare gases, discrete absorption lines of the impurity core transitions are always superimposed to the host absorption and could, therefore, not be studied for very small, i.e., microscopic impurity, concentrations ($c < 0.1$ at.%).

In contrast to this, however, microscopic impurity absorption effects could be studied in the long-wavelength region where the host crystal (e.g., Ar doped with Xe) is still transparent.[13,46] Some properties of the conduction band of the host crystal can be studied by observing the energy position of the exciton absorption lines. Other measurements on mixed systems with different concentrations have been performed on the solid rare gases in the valence-band absorption region[47] and on the alkali halides in the valence-band[48] and the core-transitions regions.[49] They have been discussed with regard to the nature of absorption peaks as excitions and interband transitions coupled to different points of the Brillouin zone.

In Sec. II we give some details of the experimental procedure. Section III summarizes the experimental results, and Sec. IV gives a discussion of our results. We will present results for (a) the Xe-4d absorption in Xe : Kr mixtures, (b) the Kr-3d absorption in Kr : Xe mixtures, (c) the Xe-4d absorption in Xe : Ar mixtures, (d) the Kr-3d absorption in Kr : N_2 mixtures, (e) the Kr-3d absorption in Kr : Ar mixtures, (f) the Ar-2p absorption in Ar : N_2 mixtures, (g) the Ne-2s absorption in Ne : Ar mixtures.

II. EXPERIMENTAL DETAILS

The experimental setup is essentially the same as was used for the thin-film absorption measurements of the pure-rare-gas solids.[1,2] It is described, to some extent, in Ref. 1. Thin-film absorption is the best method for obtaining optical constants in the energy range above 25 eV. The reflectivity in this energy range is very low and as

a result no correction for reflection losses is necessary.

The light comes from the 7.5-GeV electron synchrotron DESY.[17,18] The spectrometer used for our experiments was a 1-m Rowland-type spectrometer with grazing incidence. Two different gratings were used for the experiments: In the energy region between 60 and 100 eV, a 2400 lines/mm grating yielded an energy resolution of ~0.05 eV; at higher energies a 3600 lines/mm grating with an energy resolution of ~0.2 eV was used. The radiation detector behind the exit slit was an open magnetic-type photomultiplier (Bendix M 306). No absolute absorption values have been obtained because the thickness of the thin films was never determined. The relative accuracy of the measurements allowed us to detect changes of more than 3% in the absorptivity of the samples. The energy-calibration method based on wavelength values given for gas-absorption lines is the same as was used in Refs. 1 and 2. The resulting energy positions for the peaks in pure rare-gas solids are slightly different from the values previously found,[1,2] but are in agreement within the error limits.

The gas mixtures were evaporated *in situ* onto thin foils which are mounted on a cryostat installed between the source and the spectrometer. The mixtures were prepared by putting the appropriate amounts of the constituents in a stainless-steel pipe; the amounts were controlled by measuring the total pressure with a precision membrane vacuummeter (Datametrix Model 1014). Circulation in the pipe was necessary in order to completely mix the constituents. The mixtures were evaporated at temperatures below the sublimation temperature of both constituents (~45 °K for Xe, ~40 °K for Kr, ~20 °K for Ar, and ~7 °K for Ne) and it is assumed that the composition in the solid phase was the same as in the gas phase before evaporation. As a result the values later used for the composition of the rare-gas mixtures are the relative partial pressures of the total pressure of ~760 Torr in the mixing vessel before evaporation. The substrates were thin films (of the order of 100–1000-Å thickness) of Al, Mg, and C. Al and Mg also served as prefilters to suppress higher-order stray light.[50]

We studied the Xe-4*d* absorption between 65 and 90 eV with admixtures of Kr and Ar, the Kr-3*d* absorption between 90 and 100 eV with admixtures of Xe, N_2, and Ar, the Ar-2*p* absorption between 243 and 255 eV with admixtures of N_2, and the Ne-2*s* absorption between 45 and 49 eV with admixtures of Ar. Figure 1 shows the absorption curves of pure solid Ne, Ar, Kr, and Xe in the energy region between 25 and 350 eV. We see that in the fine-structure region of the Ne-2*s*, Xe-4*d*, Kr-3*d*, and Ar-2*p* transitions the other gases generally show a smooth continuum absorption. This is also true for N_2 over the whole energy range.[51]

If two gases would not form a dilute mixture but a solid with well-separated regions of the two components, pure additive superposition of the two absorption curves would occur and the energy position of the absorption peaks in fine-structure regions would essentially be unaffected. We will, however, see later that for many cases the absorption peaks are continuously shifted from the position in the pure material to higher or lower energies depending on the second component and the mixing ratios in the alloy. This fact indicates a complete mixing of the two components through the whole range of mixing ratios.

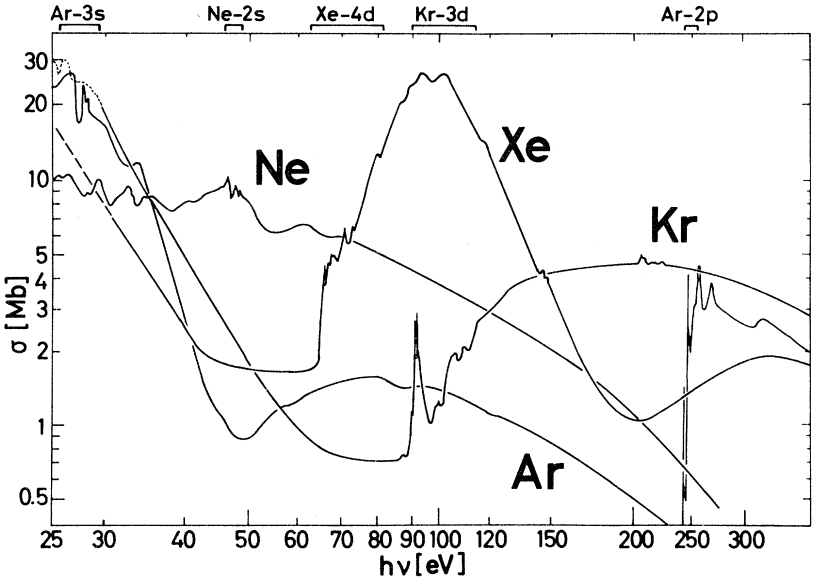

FIG. 1. Absorption curves of the pure solid rare gases Ne, Ar, Kr, and Xe compiled from the data given in Refs. 1–4. The energy ranges are indicated where the fine structure of the different solid rare gases have been studied with alloying of other rare gases and N_2.

The dilute mixing was also observed in electron diffraction patterns of the solid-rare-gas films. The diameters of the different rings in the diffraction pattern showed a smooth transition between the values of the pure components which formed the mixtures.

Only a few cases, namely Xe : Ar and Kr : N_2, were observed where, for certain concentrations, no complete mixing occurred. This was observed from the fact that the absorption peaks were found at the positions in pure Xe or Kr (for details see Sec. III).

In the electron diffraction studies we found no evidence of monocrystal structure in portions of our samples; the area of diffraction, however, was relatively large (~0.5 mm^2). We know that the optical structure, i.e., the width of the sharpest peaks depends on the temperature during evaporation.[1] At temperatures just below the sublimation temperatures we obtained peak widths which were the same as the widths of the corresponding gas absorption lines. We therefore assumed that the crystalline order was sufficient to obtain optimal line widths.

As we have mentioned before the sublimation temperature for pure Xe samples is 45 °K, but for Xe : Kr one has to evaporate below 40 °K and for Xe : Ar mixtures below 15 °K. To see the effect of temperature in pure Xe samples these were also studied at different temperatures between 40 °K and the temperature of liquid He. Evaporation at lower temperatures increases the line width, but the peak maxima can still be observed and their positions do not change when the evaporation temperature is varied.

The experimental results of the different absorption measurements are given in Figs. 2–10. The absorption curves have been obtained by dividing the transmission curves of the evaporated and the empty substrates. The final curves have been obtained from absorption curves derived from measurements with films of different thickness. This also served to check the consistency of the results. The zero of absorption has been suppressed and the absorption values are given in arbitrary units since absolute values are of no importance for the problems now under consideration. We are mainly interested in the shape and energetic positions of the different absorption maxima. For this reason the influence of stray light and higher orders was also of minor importance; both, however, were kept low by appropriate filtering with Al and Mg foils.

III. EXPERIMENTAL RESULTS

In this section we present the experimental results given in Figs. 2–10.

A. Xe-4*d* Structure in Xe : Kr Mixtures

Figure 2 shows the fine structure of the Xe-4*d* absorption in the energy range between 64 and 90 eV for different Xe : Kr mixtures with Xe content ranging from 100 to 1 at.%. Even for 1 at.% Xe, some structure can be seen because in this range the ratio of Xe and Kr absorption is especially favorable (see Fig. 1, where the absorption cross section σ of Xe in the region of 4*d* fine structure is ~6 Mb, whereas σ for Kr in the same energy range is ~0.7 Mb). The labeling of the peaks *A*, *B*, *B'*, ... , *H*, *H'* is the same as in Ref. 1. We see that by adding Kr all the peaks move to higher energies, the more the higher their energies are above threshold (~65 eV). No shift is observed for *A*; the shift of *H'* is about 2 eV. An exception to this rule

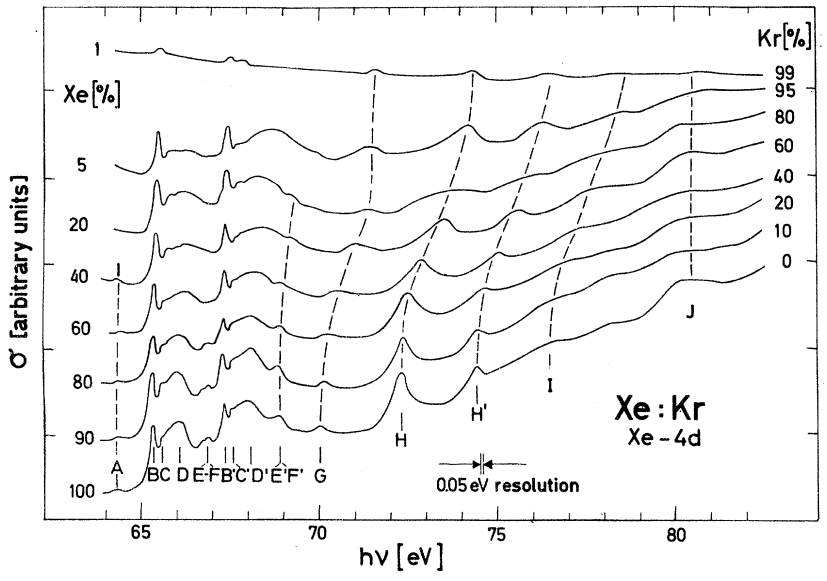

FIG. 2. Fine structure of the Xe-4*d* absorption in the energy range 64–90 eV for different Xe : Kr mixtures ranging from 100 at.% to 1 at.% Xe. The corresponding peaks are connected by dashed lines.

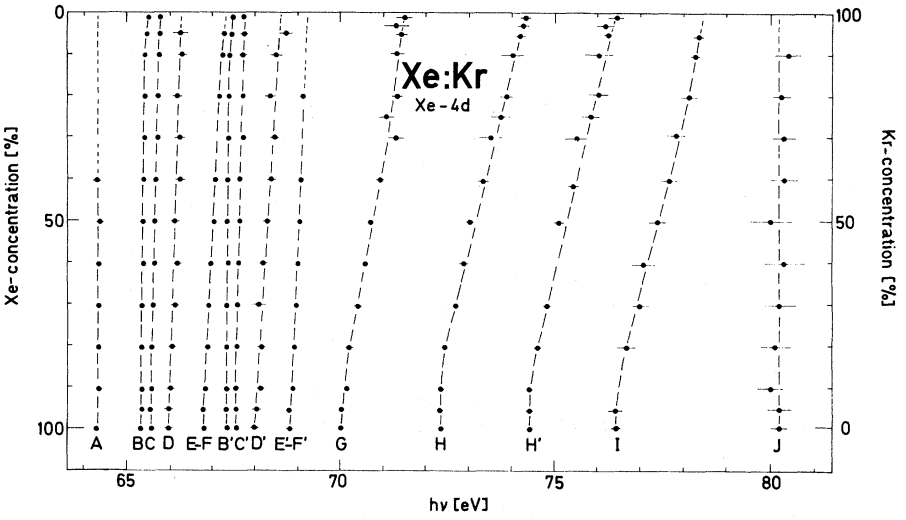

FIG. 3. Position of the different absorption peaks A–J in the Xe-4d spectrum for different concentrations of Xe : Kr mixtures. All concentrations are given in atomic percents.

is the peak J near 80 eV, which shows no shift when adding Kr. With the exception of low Kr contents ($c_{Kr} < 20$ at.%), the shift of the energy positions is proportional to the Kr concentration.

Figure 3 shows the energetic positions of the different maxima as taken from the original curves for the different Xe : Kr concentrations. The absorption spectra show transitions from the different sublevels ($J = \frac{5}{2}$ and $\frac{3}{2}$) of the Xe 4d level, which have an energy distance of ~2 eV.[52] The corresponding peaks have the same primed and unprimed roman letter. The gradient of $\Delta E/\Delta c$ depends on the energy of the peak in pure Xe, but we find the same gradient for the corresponding peaks. This supports the former assumption[1] that they are corresponding spin-orbit mates. In Ref. 1 the assignment of spin-orbit mates has come from their energy separation of ~2 eV and the similarity of their shapes. We now have the additional information that spin-orbit mates are shifted by the same amount by admixing another rare gas. The linear dependence of the peak shift on the Kr concentration allows extrapolation to $c_{Xe} = 0$ at.% or $c_{Kr} = 100$ at.%. The position of the Xe-4d peaks in 100 at.% and 0 at.% Xe is summarized in Table I. The energy shift obtained by this extrapolation procedure will be called "maximum shift" for all the alloys reported in this paper. We very clearly see that the energy shift is the same for the corresponding spin-orbit partners.

TABLE I. Energy positions of the absorption maxima in the 4d spectrum of pure solid Xe and their maximum shift in Xe : Kr and Xe : Ar mixtures (as extrapolated for $c_{Xe} = 0$ at.% and $c_{Kr,Ar} = 100$ at.%).

Peak	Pure Xe (eV)	Maximum shift in Xe : Kr mixtures (eV)	Maximum shift in Xe : Ar mixtures (eV)
A	64.3 ± 0.08	0.0 ± 0.1	0.0 ± 0.06
B	64.35 ± 0.05	+0.17 ± 0.05	+0.58 ± 0.08
B'	67.34 ± 0.05	+0.16 ± 0.05	+0.58 ± 0.08
C	65.6 ± 0.05	+0.28 ± 0.05	+0.75 ± 0.1
C'	67.58 ± 0.05	+0.25 ± 0.05	+0.80 ± 0.1
D	66.0 ± 0.1	+0.3 ± 0.1	
D'	68.0 ± 0.07	+0.65 ± 0.15	
E,F	66.8 ± 0.08	+0.55 ± 0.08	+2.2 ± 0.4
E',F'	68.8 ± 0.08	+0.42 ± 0.08	+2.5 ± 0.4
G	70.0 ± 0.05	+1.5 ± 0.15	+2.75 ± 0.3
H	72.33 ± 0.07	+2.02 ± 0.15	+3.2 ± 0.3
H'	74.4 ± 0.07	+2.04 ± 0.15	+3.2 ± 0.3
I	76.45 ± 0.08	+2.06 ± 0.15	+3.2 ± 0.3
J	80.0 ± 0.08	0.0 ± 0.08	

The fact that at certain energies peaks may be seen which result from the superposition of transitions from different spin-orbit subshells of 4d (with $J = \frac{5}{2}$ and $\frac{3}{2}$) consequently having different $\Delta E/\Delta c$ explains the disappearance of, e.g., the faster moving peaks E, F under the slower moving peak B'. The different $\Delta E/\Delta c$ within one series also explains why C, being more a shoulder of D in pure Xe, becomes more distinguishable from D with higher Kr concentrations. The same is true for C' and D'.

The situation is more entangled for C' and D'. We have to consider that the structure C', D' has contributions from different conduction band density of states.[45] It is, therefore, difficult to exactly determine the maximum shift of D' (see Table I).

B. Kr-3d Structure in Kr : Xe Mixtures

Figure 4 shows the fine structure of the Kr-3d transitions between 91 and 99 eV for different Kr : Xe concentrations. In contrast to the Xe-4d structure, we here see a shift to lower energies when Xe is added. The shift is small near the onset of transitions (B and B', which again show the same behavior as the other spin-orbit mates) and becomes larger for peaks at higher energies (e.g., G, G') so that the whole spectrum tends to contract, whereas

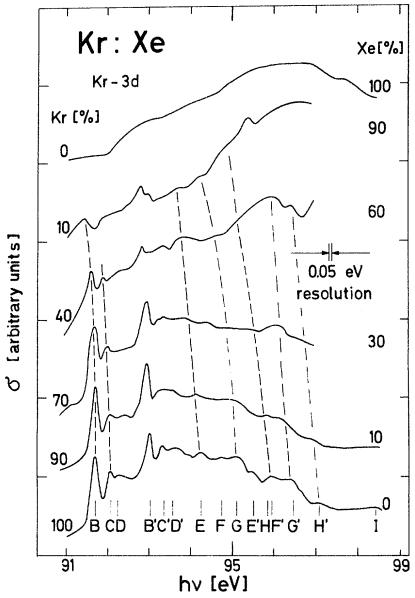

FIG. 4. Fine structure of the Kr-3*d* absorption in the energy range 90–99 eV for different Kr : Xe mixtures ranging from 100–10 at. % Kr. The curve for 100 at. % Kr is also included to explain the continuum absorption increasing towards higher photon energies for small Kr concentrations.

the Xe-4*d* spectrum in Xe : Kr mixtures expands.

The situation for identifying peaks and for following their motion to lower Kr concentrations is less favorable than for the Xe-4*d* spectrum in the Xe : Kr mixtures: (a) As can be seen from Fig. 1, the Xe absorption near 90 eV has merely a broad maximum with $\sigma \simeq 27$ Mb, whereas the Kr-3*d* fine structure ranges between 0.7 and 3 Mb. It is, therefore, difficult to observe the Kr-3*d* structure for small Kr concentrations. (b) As the whole spectrum contracts and the spin-orbit splitting energy of the Kr-3*d* shell is less than that of Xe-4*d*, namely ~1.2 eV,[52] the peaks are not so well separated from each other.

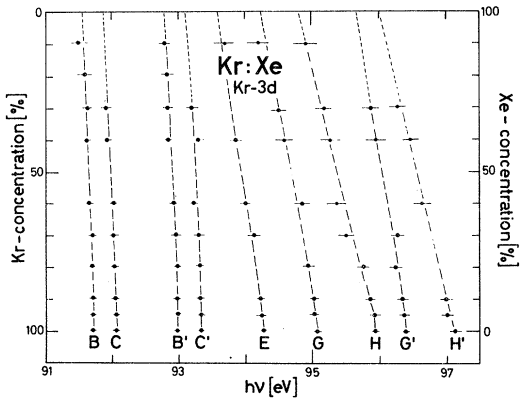

FIG. 5. Position of the different absorption peaks *B* to *H'* in the Kr-3*d* spectrum for different concentrations of Kr : Xe mixtures. Concentrations are given in atomic percents.

In Fig. 5 the peak positions for the different Kr : Xe concentrations are taken from the original spectrometer curves. We see that with the reserved sign $\Delta E/\Delta c$ increases again when going to higher energies. The extrapolation to 0 at. % Kr giving the values for the maximum shift, summarized in Table II, obviously contains a larger error than the Xe values in Table I.

C. Xe-4*d* Structure in Xe : Ar Mixtures

The fine structure of the Xe-4*d* absorption in the energy range 64–80 eV is shown again in Fig. 6, but now with alloying solid Ar. As for Xe : Kr mixtures we see a shift of the peaks to higher energies. A breaking of the systematic shift seems to occur in the curve with $c_{Xe} = 60$ at. %. At the energy position of *H* in pure Xe a peak occurs which obviously indicates at least a partial dealloying of the two components. Table I also shows the energetic positions of the different peaks for $c_{Xe} = 0$ at. % ($c_{Ar} = 100$ at. %) as obtained from the original spectrometer curves. We again find a shift proportional to the Ar content for $c_{Ar} > 20$ at. % (see Fig. 6).

A comparison of the values given in Table I shows that the shift of peaks is much larger for Ar mixtures than for Kr mixtures. Peak *A* does not shift in both cases, but for *B* (*B'*) the shift is 0.17 eV (0.16 eV) in Kr and 0.58 eV (0.58 eV) in Ar, for *C* (*C'*) the shift is 0.28 eV (0.25 eV) and 0.75 eV (0.80 eV), respectively, and finally for *H*(*H'*) and *I*

TABLE II. Energy positions of the absorption maxima in the 3*d* spectrum of pure solid Kr and their maximum shift in Kr : Xe and Kr : Ar mixtures (as extrapolated for $c_{Kr} = 0$ at. % and $c_{Xe,Ar} = 100$ at. %).

Peak	Pure Kr (eV)	Maximum shift in Kr : Xe mixtures (eV)	Maximum shift in Kr : Ar mixtures (eV)
A	90.4 ± 0.08		
B	91.73 ± 0.05	−0.14 ± 0.1	+0.38 ± 0.05
B'	93.00 ± 0.05	−0.20 ± 0.08	+0.37 ± 0.05
C	92.08 ± 0.05	−0.18 ± 0.1	+0.48 ± 0.05
C'	93.34 ± 0.05	−0.21 ± 0.1	+0.59 ± 0.05
E	94.23 ± 0.05	−0.7 ± 0.1	+0.93 ± 0.2
E'	95.45 ± 0.08		+0.93 ± 0.2
G	95.03 ± 0.06	−0.8 ± 0.25	+1.1 ± 0.2
G'	96.4 ± 0.06	−0.75 ± 0.25	+0.9 ± 0.2
H	95.85 ± 0.07	−1.1 ± 0.2	
H'	97.13 ± 0.09	−1.1 ± 0.2	
I	98.25 ± 0.1		+1.1 ± 0.3
J	98.8 ± 0.1		+1.03 ± 0.2 +2.04 ± 0.3
K	101.05 ± 0.1		+1.55 ± 0.3
K'	102.4 ± 0.15		+1.6 ± 0.4
L	106.05 ± 0.15		+0.4 ± 0.4 +1.4 ± 0.5
M	110.6 ± 0.2		+0.45 ± 0.4

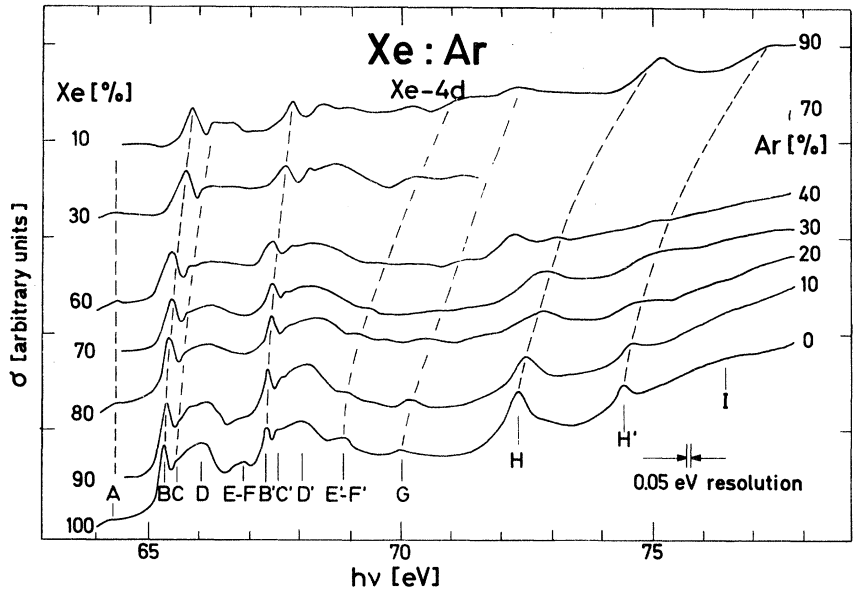

FIG. 6. Fine structure of the Xe-4*d* adsorption in the energy range 64–80 eV for different Xe : Ar mixtures ranging from 100–10 at.% Xe. The corresponding peaks are connected by dashed lines.

we obtain 2.02 eV (2.04 eV) and 2.06 eV for Kr and 3.2 eV (3.2 eV) and 3.2 eV for Ar.

It should, however, be noted that an unambiguous association of the corresponding peaks of different concentrations is much easier in the Xe : Kr system than in the Xe : Ar system. The shift of the B, B', C, C' structures in Xe : Ar is quite clear but for the higher energy peaks G, H, and H' one could also think that for $c_{Ar} = 40$ and 90 at.%, they are at just the same position as in pure Xe. This could be explained by a demixing of the system for these concentrations, but if this is so, the peaks B, B' should also be at the position in pure Xe, which is obviously not the case.

D. Kr-3*d* Structure in Kr : N_2 Mixtures

A clear case of demixing can be observed in the Kr : N_2 mixture (Fig. 7). For small N_2 concentrations one sees that the different peaks shift to higher energies, but for 40 at.% and more the Kr peaks appear again at their old positions. Here the Kr and N_2 obviously form well-separated islands in the film.

E. Kr-3*d* Structure in Kr : Ar Mixtures

Figure 8 shows the fine structure of the solid Kr-3*d* absorption in the energy range 90–100 eV with the admixing of Ar. We again find the general tendency that the peaks are shifted to higher energies. The peak shift increases the higher the peak position above threshold. Table II shows the energetic positions of the different peaks for $c_{Kr} = 0$ at.% ($c_{Ar} = 100$ at.%) as obtained from the original spectrometer curves. The shift is once more proportional to c_{Ar}, and $\Delta E/\Delta c$ is again the same for spin-orbit mates. The structures above 96 eV were only observable up to $c_{Kr} \simeq 50$–60 at.%. It seems that two of the peaks, namely J and L, split into two peaks. They are included in Table II, but not in Fig. 8, so as to avoid compression of the ab-

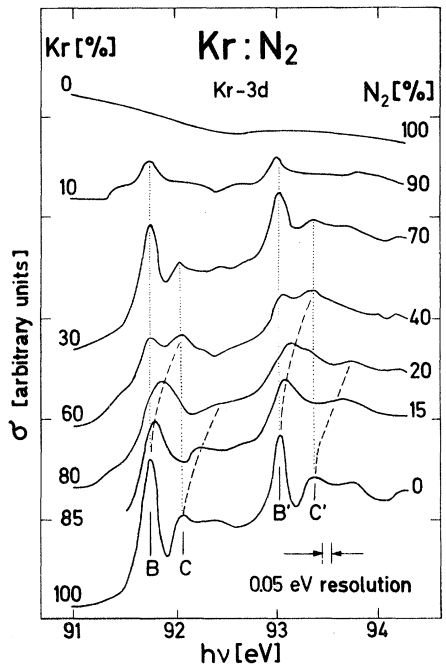

FIG. 7. Fine structure of the Kr-3*d* adsorption in the energy range 91–94.5 eV for different Kr : N_2 mixtures ranging from 100–10 at.% Kr. The curve for pure N_2 is also included. The dashed lines connect peaks in the mixed system, the dotted lines in the decomposed system.

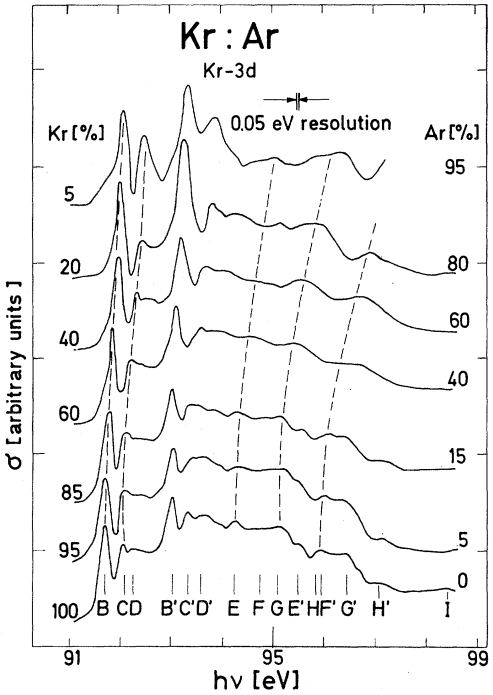

FIG. 8. Fine structure of the Kr-3*d* absorption in the energy range 90–99 eV for different Kr : Ar mixtures ranging from 100–5 at. % Kr. The corresponding peaks are connected by dashed lines.

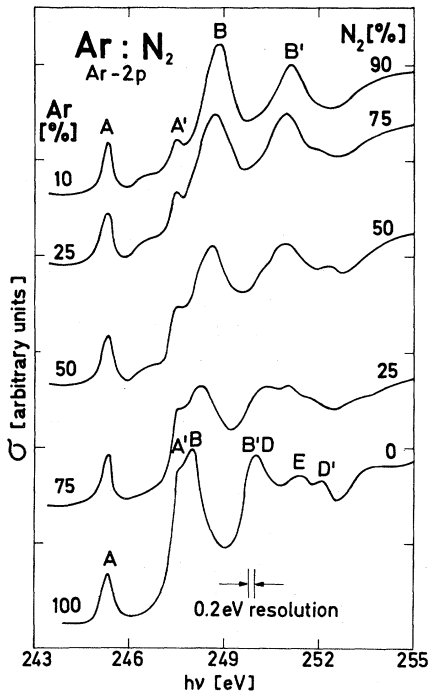

FIG. 9. Fine structure of the Ar-2*p* absorption in the energy range 243–255 eV for different Ar : N_2 mixtures ranging from 100–10 at. % Ar.

sorption features near the threshold energy. The explanation may be that they are composed of transitions from the different Kr-3*d* subshells which both shift with different amounts. The splitting of *L* may also be due to the fact that *L* is partially caused by a double excitation (see Sec. IV C).

The broad structures near 110 eV could be observed up to 80 at. % Ar. They shift much less than peaks at lower energies, as is also the case for the structures in Xe at 80.0 eV.

Another interesting feature is that the peaks *B*, *B'*, *C*, and *C'* become more and more pronounced if Ar is added.

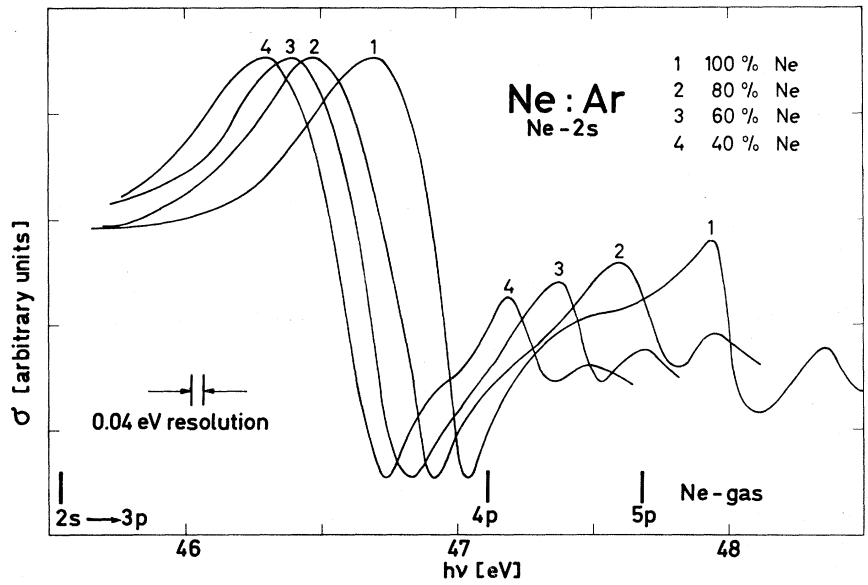

FIG. 10. Fine structure of the Ne-2*s* absorption in the energy range 45.5–48.5 eV for different Ne : Ar mixtures ranging from 100–40 at. % Ne.

F. Ar-2p Structures in Ar : N_2 Mixtures

The 2p absorption of solid Ar has been investigated in mixtures with Kr, Xe and N_2. In Ar : Kr and Ar : Xe the peaks shift to lower energies; with N_2 they shift to higher energies. Figure 9 shows the fine structure in the energy range 243–255 eV, with admixing of N_2. The results have already been mentioned in Ref. 2. In the pure Ar spectrum the spin-orbit mate of A labeled A' can only be seen as a shoulder of B. When admixing N_2 the peaks A and A' do not change their positions at 245.3 and 247.5 eV, respectively, whereas B at 248.0 eV is shifted by +1.0 eV and B' at 250.0 eV by +1.2 eV. Thus A' and B can be seen as clearly separated maxima in the Ar : N_2 mixtures.

G. Ne-2s Structures in Ne : Ar Mixtures

We would finally like to mention the results of Ne : Ar mixtures. Figure 10 shows the fine structure of the solid Ne-2s absorption in the energy range 45.5–48.5 eV, with admixing of Ar. The lines in pure solid Ne have a strongly asymmetric shape,[23] very similar to what has been found in the gas.[53] In the Ne : Ar mixtures the peaks are shifted to lower energies but the line profile character remains unchanged. Extrapolating to $c_{Ne}=0$ at.% ($c_{Ar}=100$ at.%) gives a maximum shift for the first line at 46.92 eV in pure Ne by −0.5 eV and for the second line at 48.0 eV in pure Ne by −1.1 eV.

Here is a summary of the experimental results:

(a) The different absorption peaks shift when other gases are added.

(b) If the atomic number of the admixed gas is higher the peaks shift to lower energies, if the atomic number is lower the peaks shift to higher energies.

(c) The energy shift of the absorption maxima are almost proportional to the concentration of the admixed partner.

(d) The amounts of energy shifting are small near threshold and increase the larger the distance of the maxima from threshold. Spin-orbit mates shift equally. The first peaks show an additive shift, that means, e.g., Ar shifts the Xe peaks by an amount (see Table I), which is approximately the sum of the Xe shift by Kr (Table I) and the Kr shift by Ar (Table II).

Judging only from Figs. 2, 4, 6, 7, and 8 the connection of the peaks by the dashed lines does not always look very convincing. It should, however, be noted that the absorption measurements were taken for more concentrations than indicated in Figs. 2, 4, 6, 7, and 8 and that the peaks often showed up more clearly in the original spectrometer curves. Only those prominent peaks which could easily be followed on mixing and which are discussed in Sec. IV were connected by the dashed lines and then labeled. Still some ambiguity remains with this identification.

Furthermore, other weaker structures, such as a shoulder on the low-energy side of B in Fig. 7 or a small peak between A and A' for the higher N_2 concentrations in Fig. 9 are experimentally evident but difficult to explain at present.

IV. DISCUSSION

Before we go into a detailed discussion on the mixture measurements of Sec. III we have to review some facts which have already been discussed in connection with the experimental data of the pure solid rare gases.[1–4,45]

With the exception of some lines (A and B in the Ne-2s and Ar-3s spectra and B and C in the Kr-3d and Xe-4d spectra) near the onset of transitions from the core shell, the absorption spectra can be explained as being due to density-of-states structures. These first lines, owing to their energetic position close to the first gas absorption lines, and their line shape and width comparable to that of the gas lines, can be interpreted as Frenkel excitons. Since, to some extent, the reaction of these excitonic peaks to alloying is different from that of density-of-states structures, we are going to discuss excitonic and density-of-states effects on the optical spectra of solid-rare-gas mixtures separately.

A. Excitonic Effects (Transitions near Threshold)

Figure 11 shows the absorption curve of gaseous and solid Ne-2s, Ar-3s and -2p, Kr-3d, and Xe-4d transitions in the vicinity of the first gas lines. The energy scales of the different spectra are normalized at the first gas line. The energy positions of the gas and solid state absorption lines and their relative distances are compiled in Table III. In all spectra the first strong absorption line in the solid (A in Ne and Ar, B in Kr and Xe) is at higher energies than the first gas line. By comparing the experimental spectra with the calculated curves for the joint density of states,[45] we conclude that the Frenkel excitons in Kr-3d and Xe-4d are above the interband transition threshold. This conclusion is supported by the fact that the oscillator strength of these excitons in Kr and Xe is smaller than that of the corresponding gas lines, owing to interactions with the underlying continuum. Peak A in Ar-2p, corresponding to a Frenkel exciton built from a 2p hole and an s-symmetric electron, is below the onset of interband transitions and, in contrast to B in Kr and Xe, its oscillator strength is similar to that of the gas lines. For Ne-2s and Ar-3s only the first two or three lines can be observed experimentally. No further structure, which could be compared with the density-of-states curve, can be seen. Therefore, it is hard to decide whether these peaks

are below or above threshold. This complete lack of interband transitions in the experimental curves of Ne-2*s* and Ar-3*s* transitions remains to be explained.

We now compare the position of the first solid state absorption line (*A*, *A'* in Ne and Ar; *B*, *B'* in Kr and Xe) with the position of the gas line for the case that in the solid the excited atom is surrounded by atoms of the same element (pure solid) or by atoms of a different rare gas (mixtures). In Fig. 12, on the left, we see the energy distance of the Xe-4*d* lines *B* and *B'* to the gas lines when the Xe atom is imbedded in Xe, Kr, and Ar. The energy distances are taken from Tables I and III. Further to the right in Fig. 12, for Kr-3*d*, we see the energy distance to the first Kr-3*d* gas lines for Kr in Xe, pure Kr, and Kr in Ar, as taken from Tables II and III. For Ar-3*s* only the distance from the gas line to the pure solid is included as no alloy measurements have been performed for this transition. For Ar-2*p* the distance is included for Ar in Xe, Ar in Kr, and pure Ar (Table III and data not included in Sec. III), and finally for Ne-2*s* the distance for Ne in Ar and pure Ne (see values in Sec. III and Table III).

The result is that the relative position of the first solid state absorption line depends only on the neighboring atoms and not on the isolated atom from which the transition comes; e.g., the distance of the first Frenkel exciton in solid Ar from the gas line is ~0.9 eV both for 2*p* and 3*s* transitions. The same value is found for the first Frenkel exciton in the 4*d* spectrum of Xe imbedded in Ar from the Xe gas line.

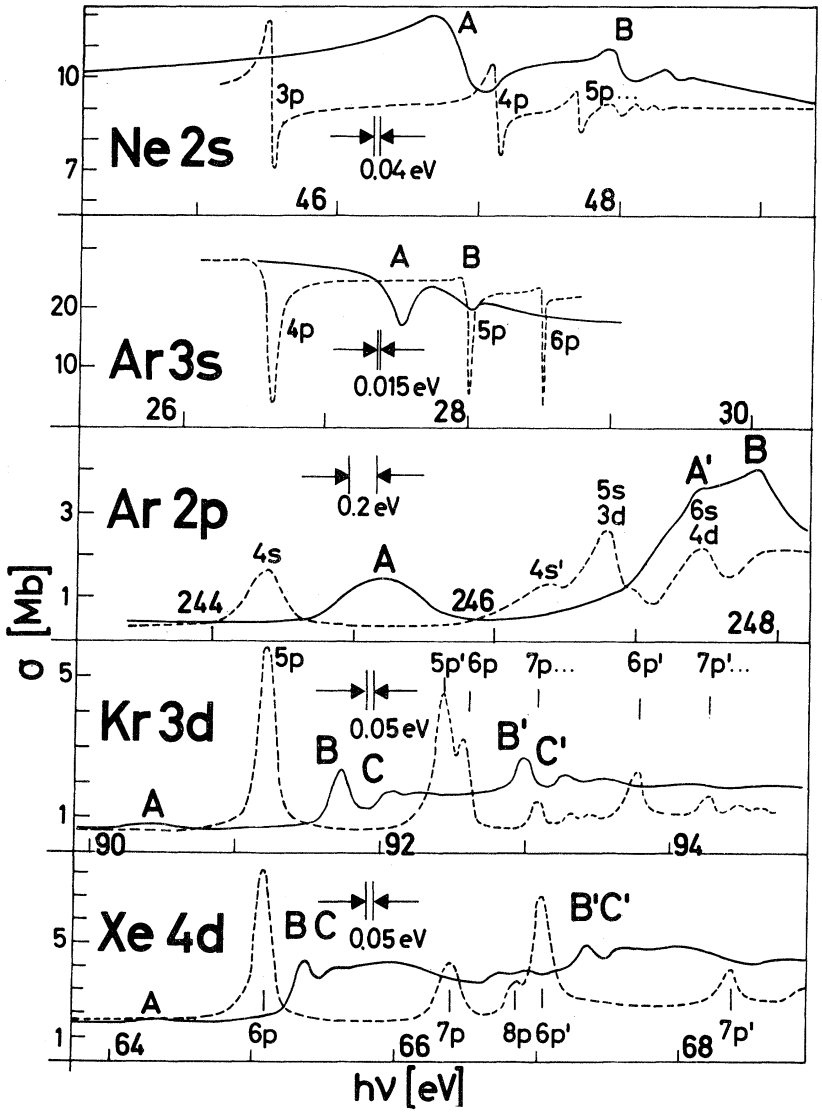

FIG. 11. The first absorption lines in gaseous (dashed lines) and solid (solid lines) Ne near the 2*s* threshold, Ar near the 3*s* and 2*p* threshold, Kr near the 3*d* threshold, and Xe near the 4*d* threshold.

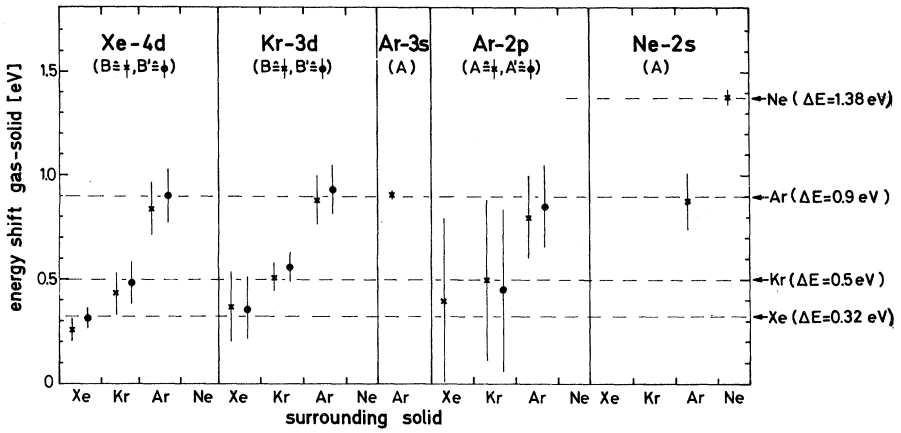

FIG. 12. Energy distance between the first solid state absorption lines and the corresponding lines in the gas for Xe-4*d*, Kr-3*d*, Ar-3*s* and -2*p*, and Ne-2*s* transitions in the pure solids and in alloys with the other rare gases.

A similar result is found for the separation of the first two absorption lines in the solid, namely $B-A$ in Ne and Ar, and $C-B$ in Kr and Xe for the pure and mixed solids (Fig. 13). On the left, for Xe-4*d*, we see the distance $C-B$ for pure Xe and for Xe in Kr and Xe in Ar, to the right follows Kr in Xe, pure Kr, and Kr in Ar, then pure Ar 3*s*, and finally Ne in Ar and pure Ne. We once more see that the energy distances of the first two absorption lines of a solid are only dependent on the neighboring atoms and not on the excited atom. The data given in Table III and Fig. 12 show that the blue shift of the first exciton with respect to the corresponding gas line increases when going from Xe to Ne. In the same way the separation of the first two exciton lines increases (Fig. 13).

Kozlenkov[54] and Kronig[55] made theoretical calculations for metal and metal alloys on the energy shift of absorption maxima with changing lattice constant a. According to these theories the shift should be proportional to $1/a^2$. Assuming $a_{\mathrm{Ne}} = 4.465$ Å, $a_{\mathrm{Ar}} = 5.315$ Å, $a_{\mathrm{Kr}} = 5.654$ Å, and $a_{\mathrm{Xe}} = 6.136$ Å one can plot E against $1/a^2$ (Fig. 14). We see that the proportionality also holds true for the solid rare gases.

B. Density-of-States Effects

The concept underlying the study of density-of-states effects on the optical spectra of solid rare gases in the far ultraviolet is the calculation of the dielectric constant in the simplified form

$$\epsilon_2(E) \sim \frac{1}{E^2} \sum_{i,f} n_{fi}(E) ,$$

neglecting the energy and $\vec{k}$ dependence of the transition matrix elements. The point density of states

$$n_{fi}(E) = \frac{1}{N} \sum_{\vec{k} \in \mathrm{BZ}} \delta(E_f(\vec{k}) - E_i(\vec{k}) - E)$$

between initial core states (i) and final conduction bands (f) is just a replica of the conduction-band density of states, because the core energy bands

TABLE III. Energy positions and relative distances of the first absorption lines in gaseous and solid Ne-2*s*, Ar-3*s* and -2*p*, Kr-3*d*, and Xe-4*d* transitions.

	J	Gas (eV)		Solid (eV)		ΔE Solid-gas (eV)		ΔE Solid (eV)	
Ne-2*s*	0	45.54 ± 0.04	$2s \rightarrow 3p$	46.92 ± 0.04	(*A*)	1.38 ± 0.04	(*A*)	1.08 ± 0.04	(*B* − *A*)
				48.0 ± 0.04	(*B*)	2.46 ± 0.04	(*B*)		
Ar-3*s*	0	26.61 ± 0.02	$3s \rightarrow 4p$	27.52 ± 0.02	(*A*)	0.91 ± 0.02	(*A*)	0.48 ± 0.02	(*B* − *A*)
				28.00 ± 0.02	(*B*)	1.39 ± 0.02	(*B*)		
Ar-2*p*	$\frac{3}{2}$	244.4 ± 0.15	$2p \rightarrow 4s$	245.2 ± 0.2	(*A*)	0.8 ± 0.2			
	$\frac{1}{2}$	246.5 ± 0.15	$2p' \rightarrow 4s'$	247.35 ± 0.2	(*A'*)	0.85 ± 0.2			
Kr-3*d*	$\frac{5}{2}$	91.22 ± 0.07	$3d \rightarrow 5p$	91.73 ± 0.05	(*B*)	0.51 ± 0.07	(*B*)	0.35 ± 0.05	(*C* − *B*)
				92.08 ± 0.05	(*C*)	0.86 ± 0.07	(*C*)		
	$\frac{3}{2}$	92.44 ± 0.07	$3d' \rightarrow 5p$	93.00 ± 0.05	(*B'*)	0.56 ± 0.07	(*B'*)	0.34 ± 0.05	(*C'* − *B'*)
				93.34 ± 0.05	(*C'*)	0.9 ± 0.07	(*C'*)		
Xe-4*d*	$\frac{5}{2}$	65.10 ± 0.02	$4d \rightarrow 6p$	65.35 ± 0.05	(*B*)	0.25 ± 0.05	(*B*)	0.25 ± 0.05	(*C* − *B*)
				65.6 ± 0.05	(*C*)	0.5 ± 0.05	(*C*)		
	$\frac{3}{2}$	67.02 ± 0.02	$4d' \rightarrow 6p'$	67.34 ± 0.05	(*B'*)	0.32 ± 0.05	(*B'*)	0.24 ± 0.05	(*C'* − *B'*)
				67.58 ± 0.05	(*C'*)	0.56 ± 0.05	(*C'*)		

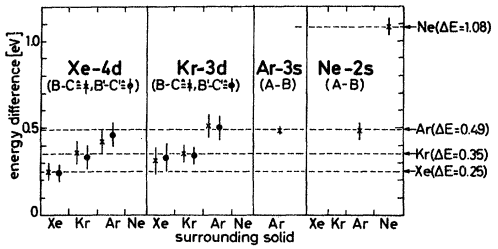

FIG. 13. Energy distance between the first two solid state absorption lines for Xe-4d, Kr-3d, Ar-3s, and Ne-2s transitions in the pure solid and in mixtures with the other rare gases.

$E_i(\vec{k})$ do not depend on $\vec{k}$. For pure-rare-gas solids[45] it has already been shown that with the exception of the excitonic peaks (A, A' in Ar-2p transitions and B, B', C, C' in Kr-3d and Xe-4d transitions) all structures in the core excitation spectra correspond to density of states. This can be seen in Fig. 15, which contains the most important results of Ref. 45. When discussing the effect of density of states on the optical spectra of dilute solid-rare-gas mixtures in the extreme ultraviolet we will make use of our knowledge of the density of states in the pure crystals.

Xe : Kr *mixtures*. As is shown in Figs. 2 and 4, the structures D, E, F, G, and H and their spin-orbit partners shift with changing composition but do not split. They may be classified as amalgamation type structures,[56] in agreement with their identification as density-of-states structures in the pure Xe or Kr spectrum.[46] Thus, what starts out as the pure Xe spectrum in the lowest curve of Fig. 2 should turn out more and more and become the pure Kr spectrum in the upper curve of Fig. 2, a spectrum which is to be understood in terms of the density-of-states structures of the Kr conduction bands. (Here of course the spin-orbit splitting of the Xe-4d as an initial state causes differences in the Kr-3d spectrum.)

Since no density-of-states calculations are available for the mixed crystals a quantitative discussion of theoretical and experimental results is only possible for the maximum shifts which are introduced in Tables I and II. If we assume that there is no shift of the core states with regard to the bottom of the conduction band, a theoretical prediction of the maximum shifts for density-of-states structures follows by comparing the position of

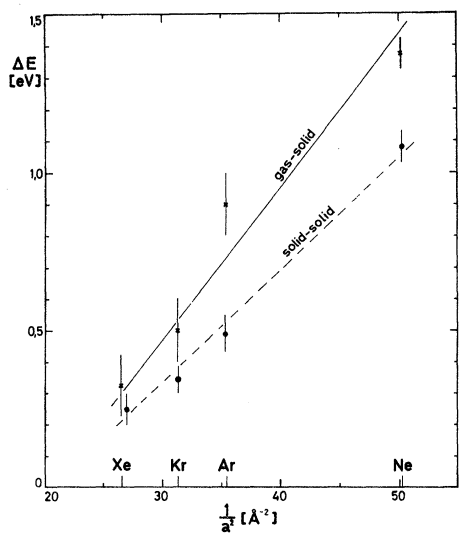

FIG. 14. Plot of the averaged energy distance from Figs. 12 and 13 vs $1/a^2$ where a is the lattice parameter.

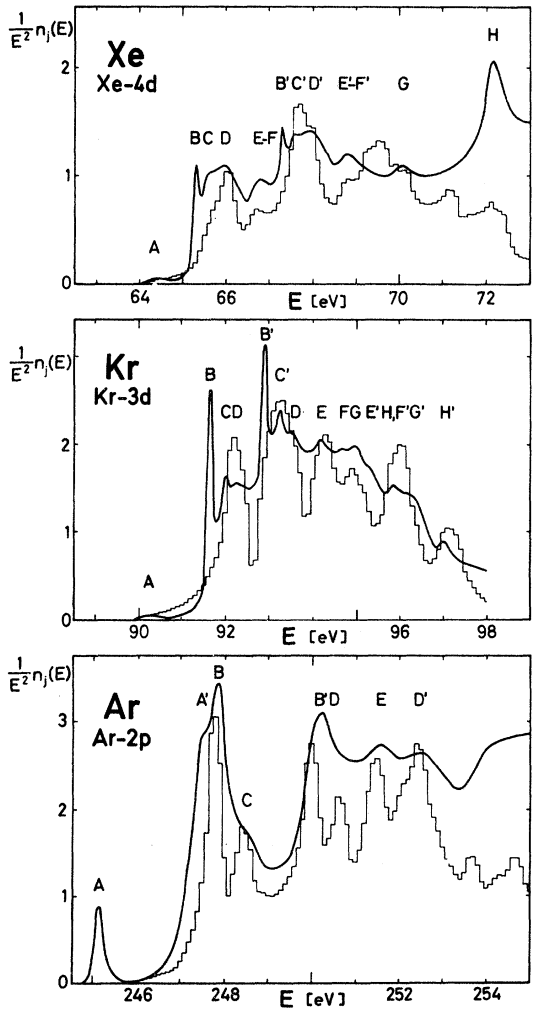

FIG. 15. Density-of-states histograms of the conduction bands of solid Ar, Kr, and Xe (essentially taken from Ref. 45, the results for Xe differ from those in Ref. 45, where the third and fourth conduction bands on the Σ axis are incorrect in comparison to the results of Ref. 39) and the experimental absorption curves as taken from Refs. 1 and 2.

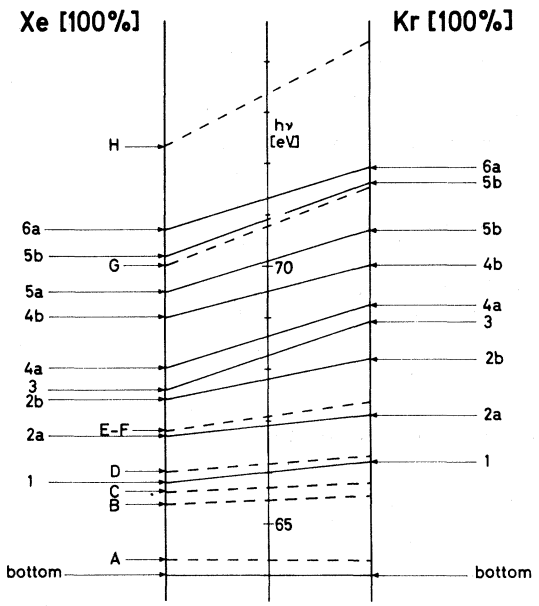

FIG. 16. Relative positions of corresponding maxima of density of states of the conduction bands 1–6 of solid Xe and Kr with respect to the bottom of the lowest conduction band (solid lines) and maximum shift (according to Table I) of the experimental peaks (dashed lines) of the Xe-4*d* absorption in Xe : Kr mixtures. a and b denote spin-orbit mates.

corresponding conduction-band density-of-states maxima in Xe and Kr with respect to the bottom of the conduction band. The theoretical shifts obtained in this way are given in Fig. 16 together with the experimental results.

The experimental values for the maximum shifts of the density-of-states maxima for the lowest conduction bands are taken from Tables I and II. Thus, the experimental maximum shift of the first conduction band is identical to that of D in Table I, which was related to the maximum of the first conduction-band density of states.[45] As we have already mentioned the maximum shift of D' is probably different from that of D because of contributions from the third conduction-band density of states. E, F, and E', F' have been interpreted as being due to the second conduction-band density of states in Xe with E' and F' also containing contributions from the fourth conduction band. Table I is also used to give the experimental maximum shift of the fifth conduction-band density-of-states maximum (G). Since the density-of-states maxima of the third and fourth conduction band in Xe contribute to more complex structures, the experimental maximum shifts can be more accurately obtained from Table II using the interpretation given for the Kr-3*d* spectrum. According to Ref. 45, peaks F and G in Fig. 4 are built up by the third Kr conduction-band density of states, whereas H and H' are caused by the density of states of the fourth conduction band of Kr.

Agreement between experimental and calculated maximum shifts of the five lowest conduction bands supports the previously given interpretation of the pure-solid-rare-gas spectra by means of density-of-states structures. Following this concept we will now discuss various mixtures.

Ar : N_2 *mixtures*. The spectra of Ar : N_2 mixtures with excitation from the Ar-2*p* level are presented in Fig. 9. Whereas in the pure Ar spectrum (lowest curve) two excitons A and A' and a variety of density-of-states structures (B, B', D, E, D') can be seen, the spectrum of the mixed crystal with $c_{Ar} = 10$ at.% ($c_{N_2} = 90$ at.%) N merely shows two doublets, A, A' and B, B'. In the pure Ar spectrum the excitonic peaks A and A' have been identified as being due to Frenkel excitons between the spin-orbit split 2*p* core states of Ar and the lowest conduction band. B and B' correspond to the density of states of the lowest conduction band and the higher energy peaks are related to the higher conduction bands in solid Ar (Ref. 45) which correspond to atomic 3*d* levels. Although we have no detailed information on the band structure of solid N_2, we do know that energy band corresponding to atomic 3*d* states of N_2 must be high up in the conduction band and cannot be involved in that part of the spectra shown in Fig. 9. Thus the upper spectrum could be interpreted as the spin-orbit split density-of-states structures B, B' corresponding to the lowest, s-symmetric conduction band in N_2 and a pair of Frenkel excitons A, A' on Ar sites.

Xe : Ar *and* Kr : Ar *mixtures*. The Xe : Ar and Kr : Ar mixtures (Figs. 6 and 8), as was also the case with the Xe : Kr mixtures, exhibit a widening of the spectra with increasing admixtures of the lighter rare gas. In contrast to this the conduction-band density of states does not follow this trend when going from Xe or Kr to Ar, e.g., the first and second density-of-states maxima are at lower energy in Ar than in Xe or Kr.[45] Thus, the concept which led to a sound interpretation of the Xe : Kr spectra does not work here with the same success. Before we offer two possible interpretations of the spectra of Figs. 6 and 8 we should mention that the shift of the higher peaks (E, F, G, H) in the Xe : Ar and Kr : Ar mixtures cannot be followed as unambiguously as was possible in the Kr : Xe and Ar : N_2 mixtures.

On the Ar side the spectra in Figs. 6 and 8 show a doublet which repeats itself at a distance equal to the core-state spin-orbit splitting. The shape of these structures and their separation from each other and from the onset of core excitation bears some resemblance to the first and second conduction-band density of states of pure Ar. The corresponding peaks in the pure Xe and Kr spectrum

do not otherwise merge into these peaks on mixing, but, on the contrary, move to higher energies.

On the other hand, an explanation of the first peaks in the upper curves of Figs. 6 and 8 by going back to B and C (B', C') in the pure Xe and Kr spectrum leaves us with the question of why the shape of the first (excitonic) peaks is so drasticly broadened on mixing.

C. Double Excitations

We should finally like to briefly comment on the nature of the high-energy structures J in Xe (Fig. 2) near 80 eV and L, M in Kr (Table II) near 110 eV. These structures do not shift at all upon mixing, or shift by an amount much smaller than an extrapolation from the absorption line behavior at smaller energies would let one expect. These peaks have been assigned[1] as due to a double excitation of the core-shell d electron and a valence p electron, in analogy to the interpretation of corresponding absorption lines in gaseous Xe and Kr at the same energy.[57] According to this interpretation the final states of both excitations are closer to the conduction-band minimum than the final state of a single excitation at the same photon energy would be.

In accordance with our general observation that the peaks shift less on mixing the closer the final state is to the conduction-band minimum, the double excitation peaks in question show only a small shift.

ACKNOWLEDGMENTS

Preliminary measurements of the Xe-4d absorption in Xe : Kr performed by P. Schreiber[3] led to the systematic studies of all mixtures described in this paper. The authors are grateful to G. Keitel for extended technical assistance and for valuable suggestions during the performance of the measurements. Thanks are also due the Deutsche Forschungsgemeinschaft for financial support.

*II Institut für Experimentalphysik der Universität Hamburg, Hamburg, Germany.

†Fachbereich Physik der Universität Marburg, Marburg, Germany.

[1]R. Haensel, G. Keitel, P. Schreiber, and C. Kunz, Phys. Rev. **188,** 1375 (1969).

[2]R. Haensel, G. Keitel, N. Kosuch, U. Nielsen, and P. Schreiber, J. Phys. (Paris) **32,** C 4-236 (1971).

[3]P. Schreiber, DESY Report No. F41-70/6 (unpublished).

[4]G. Keitel, DESY Report No. F41-70/7 (unpublished).

[5]J. W. Cooper, Phys. Rev. Lett. **13,** 762 (1964).

[6]S. T. Manson and J. W. Cooper, Phys. Rev. **165,** 126 (1968).

[7]U. Fano and J. W. Cooper, Rev. Mod. Phys. **40,** 441 (1968); Rev. Mod. Phys. **41,** 724 (1969).

[8]W. Brandt, L. Eder, and S. Lundqvist, J. Quant. Spectrosc. Radiat. Transfer **7,** 185 (1967).

[9]A. F. Starace, Phys. Rev. A **2,** 118 (1970).

[10]M. Y. Amusia, N. A. Cherepkov, and L. V. Cernysheva, Zh. Eksp. Teor. Fiz. **60,** 160 (1970) [Sov. Phys.-JETP **33,** 90 (1971)].

[11]D. J. Kennedy and S. T. Manson, Phys. Rev. A **5,** 227 (1972).

[12]Y. Toyozawa, in Proceedings of the International Conference on VUV Radiation Physics, Tokyo, 1971 (unpublished).

[13]K. Dressler, J. Quant. Spectrosc. Radiat. Transfer **2,** 683 (1962).

[14]I. T. Steinberger, C. Atluri, and O. Schnepp, J. Chem. Phys. **52,** 2723 (1970).

[15]R. Scharber and S. E. Webber, J. Chem. Phys. **55,** 3985 (1971).

[16]G. Baldini, Phys. Rev. **128,** 1562 (1962).

[17]R. Haensel and C. Kunz, Z. Angew. Phys. **23,** 276 (1967).

[18]R. P. Godwin, in *Springer Tracts on Modern Physics*, edited by G. Höhler (Springer, Berlin, 1969), Vol. 51, p. 1.

[19]R. Haensel, G. Keiterl, E. E. Koch, M. Skibowski, and P. Schreiber, Phys. Rev. Lett. **23,** 1160 (1969).

[20]R. Haensel, G. Keitel, E. E. Koch, M. Skibowski, and P. Schreiber, Opt. Commun. **2,** 59 (1970).

[21]R. Haensel, G. Keitel, E. E. Koch, N. Kosuch, and M. Skibowski, Phys. Rev. Lett. **25,** 1281 (1970).

[22]R. Haensel, G. Keitel, P. Schreiber, and C. Kunz, Phys. Rev. Lett. **22,** 398 (1969).

[23]R. Haensel, G. Keitel, C. Kunz, and P. Schreiber, Phys. Rev. Lett. **25,** 208 (1970).

[24]E. Boursey, J.-Y. Roncin, and H. Damany, Phys. Rev. Lett. **25,** 1279 (1970).

[25]H. Damany, J.-Y. Roncin, and N. Damany-Astoin, Appl. Opt. **5,** 297 (1966).

[26]J. A. Soules and C. H. Shaw, Phys. Rev. **113,** 470 (1959).

[27]E. M. Hörl and J. A. Suddeth, J. Appl. Phys. **32,** 2521 (1961).

[28]O. Bostanjoglo and L. Schmidt, Phys. Lett. **22,** 130 (1966).

[29]P. Keil, Z. Phys. **214,** 251 (1968).

[30]J. Daniels and P. Krüger, Phys. Status Solidi B **43,** 659 (1971).

[31]C. Colliex and B. Jouffrey, J. Phys. (Paris) **32,** 46 (1971).

[32]L. Schmidt, Phys. Lett. A **36,** 87 (1971).

[33]R. S. Knox and F. Bassani, Phys. Rev. **124,** 652 (1961).

[34]W. B. Fowler, Phys. Rev. **132,** 1591 (1963).

[35]L. F. Mattheis, Phys. Rev. **133,** A1399 (1964).

[36]M. H. Reilly, J. Phys. Chem. Solids **28,** 2067 (1967).

[37]R. Ramirez and L. M. Falicov, Phys. Rev. B **1,** 3464 (1970).

[38]N. O. Lipari, Phys. Status Solidi **40,** 691 (1970).

[39]U. Rössler, Phys. Status Solidi **42,** 345 (1970).

[40]N. O. Lipari and W. B. Fowler, Phys. Rev. B **2,** 3354 (1970).

[41]N. O. Lipari, A. B. Kunz, and W. B. Fowler, Phys. Status Solidi B **45,** K43 (1971).

[42]L. Dagens and F. Perrot, Phys. Rev. B **5,** 641 (1972).

[43]R. S. Knox, *The Theory of Excitons* (Academic, New York, 1963).

[44]U. Rössler, in *Computational Solid State Physics*, edited by F. Herman, N. W. Dalton, and T. R. Koehler (Plenum, New York, 1972), p. 161.

[45]U. Rössler, Phys. Status Solidi B **45,** 483 (1971).

[46]G. Baldini and R. S. Knox, Phys. Rev. Lett. **11,** 127 (1963); G. Baldini, Phys. Rev. **137,** A508 (1965); J.-Y. Roncin, N. Damany, and J. Romand, J. Mol. Spectrosc. **22,** 154 (1967); J.-Y. Roncin, V. Chandrasekharan, N. Damany, and B. Vodar, J. Chim. Phys. **60,** 1212 (1960).

[47]N. Nagasawa, T. Karasawa, N. Miura, and T. Nanba, J. Phys. Soc. Jap. **32,** 1155 (1972).

[48]W. Martienssen, J. Phys. Chem. Solids **2,** 257 (1957); H. Mahr, Phys. Rev. **122,** 1464 (1961); H. Saito, S. Saito, and R. Onaka, J. Phys. Soc. Jap. **27,** 126 (1969); M. Watanabe, Y. Nakamura, Y. Nakai, and T. Murata, J. Phys. Soc. Jap. **26,** 1014 (1969).

[49]Y. Nakamura, M. Watanable, S. Sato, and Y. Nakai (unpublished).

[50]J. A. R. Samson, *Techniques of Vacuum Ultraviolet Spectroscopy* (Wiley, New York, 1967).

[51]Unpublished DESY results.
[52]K. Codling and R. P. Madden, Phys. Rev. Lett. **12**, 106 (1964).
[53]K. Codling, R. P. Madden, and D. L. Ederer, Phys. Rev. **155**, 26 (1967).
[54]A. I. Kozlenkov, Izv. Akad. Nauk SSSR 25, 957 (1961)[Bull. Acad. Sci. USSR Phys. Ser. 25, 989 (1961)].
[55]R. Kronig, Z. Phys. **70**, 317 (1931); Z. Phys. **75**, 191 (1932).
[56]Y. Onodera and Y. Toyozawa, J. Phys. Soc. Jap. **24**, 341 (1968).
[57]K. Codling and R. P. Madden, Appl. Opt. **4**, 1431 (1965).

PHYSICAL REVIEW B VOLUME 7, NUMBER 4 15 FEBRUARY 1973

Quantum-Mechanical Calculations of the Infrared Properties of H^- Ions in Potassium Halides*

R. F. Wood
Solid State Division, Oak Ridge National Laboratory, Oak Ridge, Tennessee 37830
and
B. N. Ganguly
Department of Physics and Materials Research Laboratory, University of Illinois, Urbana, Illinois 61801
(Received 19 June 1972)

The infrared properties of the H^- ion in KCl, KBr, and KI are studied using force constants obtained from quantum-mechanical calculations of the electronic structure of the U center. The anharmonic sidebands of the H^- local mode and the induced far-infrared absorption are calculated. In most cases the calculated force-constant changes give results comparable to the parametrized values used in previous work. It is emphasized that the force-constant changes in A_{1g}, E_g, and T_{1u} displacements are not generally equal. Occasionally, features not found in previously published experimental or theoretical work are observed. Repulsive Born–Mayer potentials for the H^--K^+ interaction in the three crystals are extracted from the quantum-mechanical calculations. Our techniques for handling the numerical evaluation of Green's functions are discussed briefly.

I. INTRODUCTION

Substitutional H^- ions (U centers) in alkali halide crystals have both ultraviolet[1] and infrared[2] absorption bands associated with them. The vibrational properties of crystals containing U centers have proved to be especially interesting. The H^- ion oscillates in a localized mode at a frequency well above that of the highest in-band mode. Sidebands[2,3] containing pronounced structure accompany the local-mode absorption. Since the H^- ions destroy the translational invariance of the host crystal, absorption also occurs in the in-band region of the spectrum.[4] Because of the light mass of H^- compared with the negative ions of the host crystal, the U center was quickly recognized as an interesting system on which to test various aspects of the theory of localized perturbations.[5,6] The first calculations[7–9] of the local-mode frequency treated the H^- ion in the mass-defect approximation. Later calculations[10–12] showed that force-constant changes must also be considered in order to explain both the local-mode frequency and the structure in the sidebands. In all of these calculations the force-constant changes were treated as adjustable parameters. However, good agreement with both the ultraviolet absorption and the infrared (ir) local-mode frequency has been obtained from first-principles quantum-mechanical calculations of the electronic structure of the U center.[13] A substitutional H^- ion in an alkali halide is particularly well suited for this type of calculation because it has relatively simple electronic structure and the same charge as that of the replaced ion, so that problems associated with electronic polarization and lattice relaxation are not insurmountable.

The primary purpose of the work described in this paper was to investigate the extent to which force constants calculated from first principles can explain the infrared properties of the U center. We have also studied the applicability of a Brillouin-zone integration technique described recently[14] to the numerical calculation of phonon Green's functions, and we shall comment briefly on this. For these purposes we have calculated the structure in the sidebands of the H^- local-mode frequency and the in-band absorption in the far-ir region. It should be clearly understood in advance that our calculations do not improve on the already excellent fit achieved in the most recent parametrized calculations,[15] although they do suggest some features not observed in previous experimental or theoretical work. One interesting by-product of